Available online at www.sciencedirect.com
SCIENCE DIRECT®
International Journal of Heat and Mass Transfer 47 (2004) 4649–4657
International Journal of HEAT and MASS TRANSFER
www.elsevier.com/locate/ijhmt

Lattice Boltzmann simulation of droplet collision dynamics

T. Inamuro *, S. Tajima, F. Ogino

Department of Chemical Engineering, Kyoto University, Katsura Campus, Kyoto 615-8510, Japan

Received 31 March 2003
Available online 8 June 2004

Abstract

A lattice Boltzmann method for two-phase fluid flows with large density ratios is presented. The method is applied to the simulations of binary droplet collisions for various Weber numbers of $20 < We < 80$ and for impact parameters of $0 \leqslant B < 0.82$ at the Reynolds number of $Re = 2000$. Two droplets with the same diameter are considered. The density ratio of the liquid to the gas is fixed at 50. Coalescence collision and two different types of separating collisions, namely reflexive and stretching separations, are simulated. The boundaries between the coalescence collision and both of the separating collisions are found and compared with an available theoretical prediction in good agreement. The mixing processes during separating collisions are also simulated for various impact parameters at $We \approx 80$, and the relation between the mixing rate and the impact parameter is obtained.

1. Introduction

The phenomena of binary droplet collision are of fundamental importance in the studies of raindrop formation, spraying processes, dispersed phase systems, and so on. Therefore, many investigations of the binary droplet collision dynamics have been performed by using experimental, numerical, and theoretical approaches [1–5]. In particular, numerical simulations are currently in progress to enhance the physical understanding of fluid dynamics inside the droplets which cannot be readily studied experimentally [6]. However, the numerical simulation of multiphase flows is a challenging subject due to the difficulty in the tracking of interfaces, the mass conservation of each fluid, and the treatments of large density ratio and surface tension.

Recently, the lattice Boltzmann method (LBM) has been developed into an alternative and promising numerical scheme for simulating multicomponent fluid flows. Gunstensen et al. [7] developed a multicomponent LBM based on the two-component lattice gas model. Shan and Chen [8] proposed an LBM model with microscopic interactions for multiphase and multicomponent fluid flows. Swift et al. [9] developed an LBM model for multiphase and multicomponent fluid flows using the free-energy approach. He et al. [10] proposed a new lattice Boltzmann multiphase model using the kinetic equation for multiphase flow. Inamuro et al. [11,12] have also proposed a lattice Boltzmann method for multicomponent immiscible fluids with the same density. The LBM has great advantages over conventional methods for multiphase flows. It does not track interfaces, but can maintain sharp interfaces without any artificial treatments. Also, the LBM is accurate for the mass conservation of each component fluid. Although the LBM is a promising method for multicomponent fluid flows, one of disadvantages is that all above schemes are limited to small density ratios less than 10. Usually the density ratio of liquid–gas systems is larger than 100, e.g., the density ratio of water to air is about 1000:1.

The aim of the present paper is to present an LBM for two-phase fluid flows with large density ratios and to apply the method to the simulations of binary droplet collisions. The difficulty in the treatment of large density ratio is resolved by using the projection method [13]. Two particle velocity distribution functions are used.

* Corresponding author. Tel.: +81-75-753-5791; fax: +81-75-753-4947.
E-mail address: inamuro@kuaero.kyoto-u.ac.jp (T. Inamuro).

0017-9310/$ - see front matter © 2004 Elsevier Ltd. All rights reserved.
doi:10.1016/j.ijheatmasstransfer.2003.08.030

Nomenclature

a	free parameter determining ϕ
b	free parameter determining ϕ
B	impact parameter, X/D
c	characteristic particle speed
$\boldsymbol{c}_i$	particle velocity
D	diameter of droplet
E_i	constants in equilibrium distribution functions
F_i	constants in equilibrium distribution functions
f_i	particle velocity distribution function for an order parameter
f_i^{eq}	equilibrium distribution function for f_i
g_i	particle velocity distribution function for a multicomponent fluid
g_i^{eq}	equilibrium distribution function for g_i
h_i	particle velocity distribution function for pressure
H_i	constants in equilibrium distribution functions
L	characteristic length
p	pressure
p_0	function determining ϕ
Re	Reynolds number, $\rho_{\mathrm{L}}DV/\mu_{\mathrm{L}}$
Sh	Strouhal number, U/c
t	time
t_0	characteristic time scale, L/U
T	free parameter determining ϕ
$\boldsymbol{u}$	current velocity of a multicomponent fluid
$\boldsymbol{u}^*$	predicted velocity of a multicomponent fluid
U	characteristic flow speed
V	relative velocity of binary collision
We	Weber number, $\rho_{\mathrm{L}}DV^2/\sigma$
$\boldsymbol{x}$	Cartesian coordinates, (x, y, z)
X	distance from the center of one droplet to the relative velocity vector on the center of the other droplet

Greek symbols

$\delta_{\alpha\beta}$	Kronecher delta
Δx	lattice spacing
Δt	time step
κ_f	constant parameter determining the width of interface
κ_g	constant parameter determining the strength of surface tension
μ	viscosity
ρ	density
ρ_0	reference density
σ	surface tension
τ_f	relaxation time for f_i
τ_g	relaxation time for g_i
τ_h	relaxation time for h_i
ϕ	order parameter representing an interface

Subscripts

G	gas phase
L	liquid phase
α	Cartesian coordinates
β	Cartesian coordinates
γ	Cartesian coordinates

One is used for the calculation of an order parameter which represents the difference between two phases, and the other is used for the calculation of a predicted velocity of the two-phase fluid without a pressure gradient. The current velocity can be obtained by using the relation between the velocity and the pressure correction which is determined by solving the Poisson equation. Binary droplet collisions with the same size droplets are calculated for various Weber numbers and impact parameters. The calculated results are classified into coalescence collision and two different types of separating collisions, namely reflexive and stretching separations, and the boundaries of three types of collisions are compared with an available theoretical prediction. The mixing processes during separating collisions are also simulated for various impact parameters, and the relation between the mixing rate and the impact parameter is obtained.

2. Numerical method

Non-dimensional variables, which are defined by using a characteristic length L, a characteristic particle speed c, a characteristic time scale $t_0 = L/U$ where U is a characteristic flow speed, and a reference density ρ_0, are used as in [14]. In the LBM, a modeled fluid, composed of identical particles whose velocities are restricted to a finite set of N vectors $\boldsymbol{c}_i$ ($i = 1, 2, \cdots, N$), is considered. The 15-velocity model ($N = 15$) is used in the present paper. The velocity vectors of this model are given by

$$[\boldsymbol{c}_1, \boldsymbol{c}_2, \boldsymbol{c}_3, \boldsymbol{c}_4, \boldsymbol{c}_5, \boldsymbol{c}_6, \boldsymbol{c}_7, \boldsymbol{c}_8, \boldsymbol{c}_9, \boldsymbol{c}_{10}, \boldsymbol{c}_{11}, \boldsymbol{c}_{12}, \boldsymbol{c}_{13}, \boldsymbol{c}_{14}, \boldsymbol{c}_{15}] = \begin{bmatrix} 0 & 1 & 0 & 0 & -1 & 0 & 0 & 1 & -1 & 1 & 1 & -1 & 1 & -1 & -1 \\ 0 & 0 & 1 & 0 & 0 & -1 & 0 & 1 & 1 & -1 & 1 & -1 & -1 & 1 & -1 \\ 0 & 0 & 0 & 1 & 0 & 0 & -1 & 1 & 1 & 1 & -1 & -1 & -1 & -1 & 1 \end{bmatrix}. \tag{1}$$

The physical space is divided into a cubic lattice, and the evolution of particle population at each lattice site is computed. Two particle velocity distribution functions, f_i and g_i, are used. The function f_i is used for the calculation of an order parameter which represents the difference between two phases, and the function g_i is used for the calculation of a predicted velocity of the two-phase fluid without a pressure gradient. The evolution of the particle distribution functions $f_i(\boldsymbol{x},t)$ and $g_i(\boldsymbol{x},t)$ with velocity $\boldsymbol{c}_i$ at the point $\boldsymbol{x}$ and at time t is computed by the following equations:

$$f_i(\boldsymbol{x}+\boldsymbol{c}_i\Delta x, t+\Delta t) = f_i(\boldsymbol{x},t) - \frac{1}{\tau_f}[f_i(\boldsymbol{x},t) - f_i^{\mathrm{eq}}(\boldsymbol{x},t)], \tag{2}$$

$$\begin{aligned} &g_i(\boldsymbol{x}+\boldsymbol{c}_i\Delta x, t+\Delta t) \\ &\quad = g_i(\boldsymbol{x},t) - \frac{1}{\tau_g}[g_i(\boldsymbol{x},t) - g_i^{\mathrm{eq}}(\boldsymbol{x},t)] \\ &\qquad + 3E_i c_{i\alpha}\frac{1}{\rho}\left[\frac{\partial}{\partial x_\beta}\mu\left(\frac{\partial u_\beta}{\partial x_\alpha}+\frac{\partial u_\alpha}{\partial x_\beta}\right)\right]\Delta x, \end{aligned} \tag{3}$$

where f_i^{eq} and g_i^{eq} are equilibrium distribution functions, τ_f and τ_g are dimensionless single relaxation times, Δx is a spacing of the cubic lattice, Δt is a time step during which the particles travel the lattice spacing, and the other variables, ρ, μ and $\boldsymbol{u}$, and constants E_i are defined below.

The order parameter ϕ representing the difference between two phases and the predicted velocity $\boldsymbol{u}^*$ of the two-phase fluid are defined in terms of the two particle velocity distribution functions as follows:

$$\phi = \sum_{i=1}^{15} f_i, \tag{4}$$

$$\boldsymbol{u}^* = \sum_{i=1}^{15} \boldsymbol{c}_i g_i. \tag{5}$$

The equilibrium distribution functions in Eqs. (2) and (3) are given by

$$\begin{aligned} f_i^{\mathrm{eq}} &= H_i\phi + F_i\left[p_0 - \kappa_f\phi\frac{\partial^2\phi}{\partial x_\alpha^2} - \frac{\kappa_f}{6}\left(\frac{\partial\phi}{\partial x_\alpha}\right)^2\right] \\ &\quad + 3E_i\phi c_{i\alpha}u_\alpha + E_i\kappa_f G_{\alpha\beta}(\phi)c_{i\alpha}c_{i\beta}, \end{aligned} \tag{6}$$

$$\begin{aligned} g_i^{\mathrm{eq}} &= E_i\left[1 + 3c_{i\alpha}u_\alpha - \frac{3}{2}u_\alpha u_\alpha + \frac{9}{2}c_{i\alpha}c_{i\beta}u_\alpha u_\beta\right. \\ &\quad \left. + \frac{3}{2}\left(\tau_g - \frac{1}{2}\right)\Delta x\left(\frac{\partial u_\beta}{\partial x_\alpha}+\frac{\partial u_\alpha}{\partial x_\beta}\right)c_{i\alpha}c_{i\beta}\right] \\ &\quad + E_i\frac{\kappa_g}{\rho}G_{\alpha\beta}(\rho)c_{i\alpha}c_{i\beta} - \frac{2}{3}F_i\frac{\kappa_g}{\rho}\left(\frac{\partial\rho}{\partial x_\alpha}\right)^2, \end{aligned} \tag{7}$$

where

$$\begin{aligned} &E_1 = 2/9, E_2 = E_3 = E_4 = \cdots = E_7 = 1/9, \\ &E_8 = E_9 = E_{10} = \cdots = E_{15} = 1/72, \\ &H_1 = 1, H_2 = H_3 = H_4 = \cdots = H_{15} = 0, \\ &F_1 = -7/3, F_i = 3E_i (i = 2,3,4,\cdots,15) \end{aligned} \tag{8}$$

and

$$G_{\alpha\beta}(\phi) = \frac{9}{2}\frac{\partial\phi}{\partial x_\alpha}\frac{\partial\phi}{\partial x_\beta} - \frac{3}{2}\frac{\partial\phi}{\partial x_\gamma}\frac{\partial\phi}{\partial x_\gamma}\delta_{\alpha\beta}, \tag{9}$$

with $\alpha,\beta,\gamma = x,y,z$ (subscripts α,β, and γ represent Cartesian coordinates and the summation convention is used). In the above equations, $\delta_{\alpha\beta}$ is the Kronecker delta, κ_f is a constant parameter determining the width of the interface, and κ_g is a constant parameter determining the strength of the surface tension. In Eq. (6), p_0 is given by

$$p_0 = \phi T\frac{1}{1-b\phi} - a\phi^2, \tag{10}$$

where a, b, and T are free parameters determining the maximum and minimum values of the order parameter ϕ. It is noted that f_i^{eq} is the same as that of the Swift et al. model [9]. The following finite-difference approximations are used to calculate the derivatives in Eqs. (6), (7), (9):

$$\frac{\partial\psi}{\partial x_\alpha} \approx \frac{1}{10\Delta x}\sum_{i=2}^{15} c_{i\alpha}\psi(\boldsymbol{x}+\boldsymbol{c}_i\Delta x), \tag{11}$$

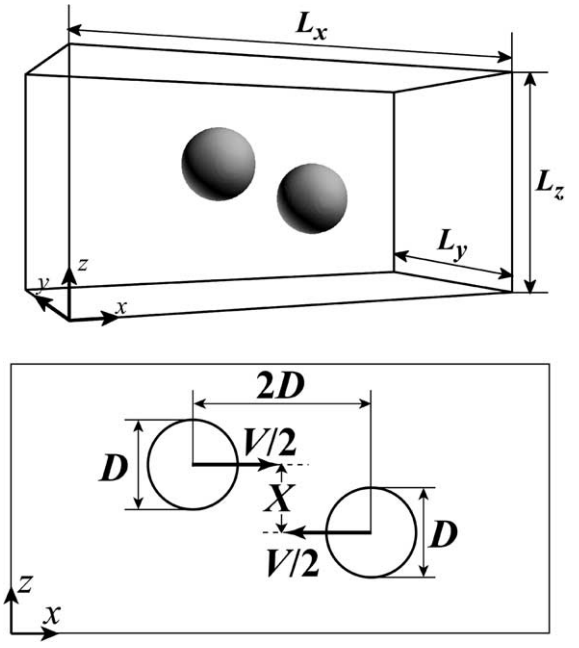

Fig. 1. Computational domain and binary droplet collision.

$$\nabla^2\psi \approx \frac{1}{5\Delta x}\left[\sum_{i=2}^{15}\psi(\boldsymbol{x}+\boldsymbol{c}_i\Delta x) - 14\psi(\boldsymbol{x})\right]. \tag{12}$$

The density in the interface is obtained by using the cut-off values of the order parameter, ϕ_{L}^* and ϕ_{G}^*, for the liquid and gas phases with the following relation:

$$\rho = \begin{cases} \rho_{\mathrm{G}}, & \phi < \phi_{\mathrm{G}}^*, \\ \frac{\Delta\rho}{2}\left[\sin\left(\frac{\phi-\overline{\phi^*}}{\Delta\phi^*}\pi\right)+1\right]+\rho_{\mathrm{G}}, & \phi_{\mathrm{G}}^* \leqslant \phi \leqslant \phi_{\mathrm{L}}^*, \\ \rho_{\mathrm{L}}, & \phi > \phi_{\mathrm{L}}^*, \end{cases} \tag{13}$$

where ρ_{G} and ρ_{L} are the density of gas and liquid phase, respectively, $\Delta\rho = \rho_{\mathrm{L}} - \rho_{\mathrm{G}}$, $\Delta\phi^* = \phi_{\mathrm{L}}^* - \phi_{\mathrm{G}}^*$, and $\overline{\phi^*} = (\phi_{\mathrm{L}}^* + \phi_{\mathrm{G}}^*)/2$.

The viscosity μ in the interface is obtained by

$$\mu = \frac{\rho-\rho_{\mathrm{G}}}{\rho_{\mathrm{L}}-\rho_{\mathrm{G}}}(\mu_{\mathrm{L}}-\mu_{\mathrm{G}}) + \mu_{\mathrm{G}}, \tag{14}$$

where μ_{G} and μ_{L} are the viscosity of gas and liquid phase, respectively.

The surface tension σ is given by

$$\sigma = \kappa_g \int_{-\infty}^{\infty}\left(\frac{\partial\rho}{\partial\xi}\right)^2 d\xi, \tag{15}$$

with ξ being the coordinate normal to the interface [15,16].

Since $\boldsymbol{u}^*$ is not divergence free ($\nabla\cdot\boldsymbol{u}^* \neq 0$), the correction of $\boldsymbol{u}^*$ is required. The current velocity $\boldsymbol{u}$ which satisfies the continuity equation ($\nabla\cdot\boldsymbol{u} = 0$) can be obtained by using the following equations:

$$Sh\frac{\boldsymbol{u}-\boldsymbol{u}^*}{\Delta t} = -\frac{\nabla p}{\rho}, \tag{16}$$

$$\nabla\cdot\left(\frac{\nabla p}{\rho}\right) = Sh\frac{\nabla\cdot\boldsymbol{u}^*}{\Delta t}, \tag{17}$$

where $Sh = U/c$ is the Strouhal number and p is the pressure. The Poisson equation (17) can be solved by various methods. In the present paper, we solve Eq. (17) in the framework of LBM. Namely, the following evolution equation of the velocity distribution function h_i is used for the calculation of the pressure p:

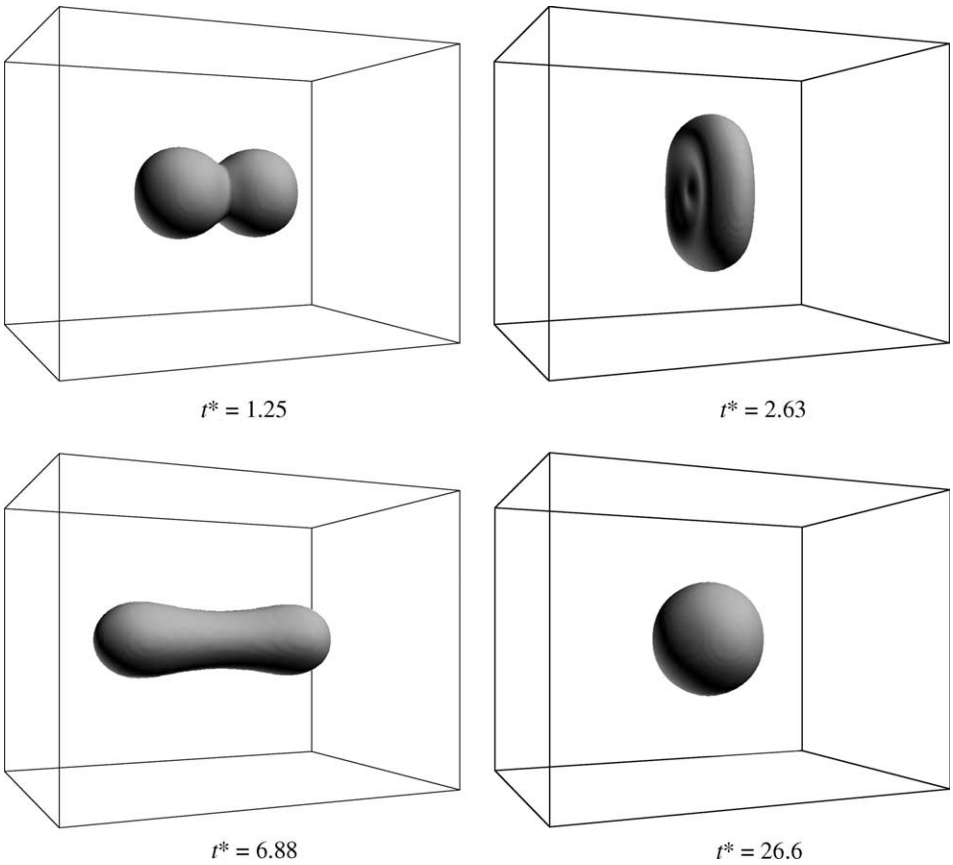

Fig. 2. Time evolution of droplet shape for $We = 20.2$ and $B = 0$ ($t^* = tV/D$).

$$h_i^{n+1}(\boldsymbol{x}+\boldsymbol{c}_i\Delta x) = h_i^n(\boldsymbol{x}) - \frac{1}{\tau_h}\left[h_i^n(\boldsymbol{x}) - E_i p^n(\boldsymbol{x})\right] - \frac{1}{3}E_i\frac{\partial u_\alpha^*}{\partial x_\alpha}\Delta x, \tag{18}$$

where n is the number of iterations and the relaxation time τ_h is given by

$$\tau_h = \frac{1}{\rho} + \frac{1}{2}. \tag{19}$$

The pressure is obtained by

$$p = \sum_{i=1}^{15} h_i. \tag{20}$$

The iteration of Eq. (18) is repeated until $|p^{n+1} - p^n|/\rho < 10^{-5}$ is satisfied in the whole domain.

Applying the asymptotic theory [14] to Eqs. (2), (3), (18), we find that the asymptotic expansions of macroscopic variables, ϕ, ρ, $\boldsymbol{u}$, and p, satisfy the phase-field advection–diffusion equation (the Cahn–Hilliard equation with advective transport) for ϕ, the continuity equation, and the Navier–Stokes equations for incompressible two-phase fluid with relative errors of $O[(\Delta x)^2]$ [17].

It is found in preliminary calculations that using the present method we can simulate two-phase flows with the density ratio up to 1000, but the iteration of Eq. (18) needs more computation time as the increase of the density ratio. In the following calculations, therefore, we use the density ratio of $\rho_L/\rho_G = 50$ for which the effect of the gas phase on the liquid phase is fairly small.

3. Results and discussion

The binary droplet collision dynamics is investigated by using the present method. Two liquid droplets with the same diameter D are placed $2D$ apart in a gas phase, and they collide with the relative velocity V (see Fig. 1). The density ratio of the liquid to the gas is $\rho_L/\rho_G = 50$ ($\rho_L = 50$, $\rho_G = 1$). The viscosities of the droplet and the gas are $\mu_L = 8 \times 10^{-2}\Delta x$ and $\mu_G = 1.6 \times 10^{-3}\Delta x$, respectively. The dimensionless parameters for binary droplet collisions are the Weber number $We = \rho_L DV^2/\sigma$, the Reynolds number $Re = \rho_L DV/\mu_L$, and the impact

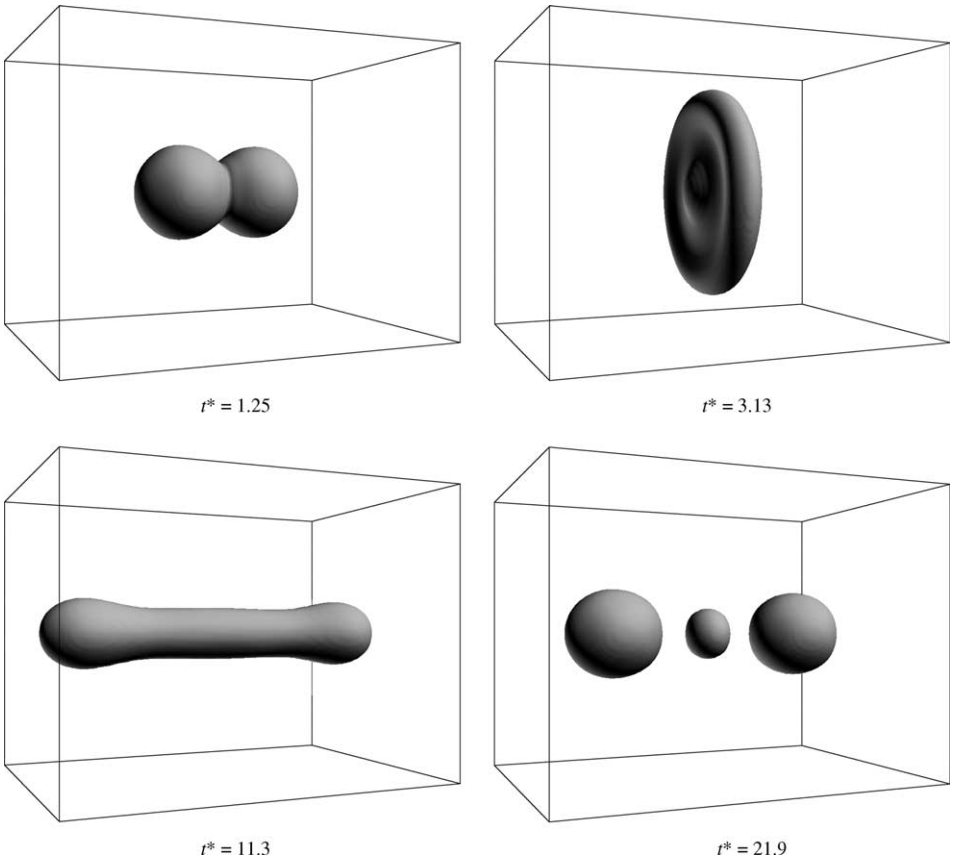

Fig. 3. Time evolution of droplet shape for $We = 78.6$ and $B = 0$ ($t^* = tV/D$).

parameter $B = X/D$, where X is the distance from the center of one droplet to the relative velocity vector placed on the center of the other droplet (see Fig. 1). The periodic boundary condition is used on all the sides of the domain. The half of the domain is calculated using the symmetry with $y = L_y/2$. The half domain is divided into a 192(or 128)×48×96 cubic lattice. The parameters in Eq. (9) are $a = 1$, $b = 6.7$, and $T = 3.5 \times 10^{-2}$; it follows that the maximum and minimum values of the order parameter are $\phi_{\max} = 9.714 \times 10^{-2}$ and $\phi_{\min} = 1.134 \times 10^{-2}$. The cut-off values of the order parameter are $\phi_{\mathrm{L}}^* = 9.2 \times 10^{-2}$ and $\phi_{\mathrm{G}}^* = 1.5 \times 10^{-2}$. The other parameters are fixed at $V = 0.1$, $\kappa_f = 0.5(\Delta x)^2$, $\tau_f = 1$, $\tau_g = 1$ and $D = 32\Delta x$, and κ_g is changed in the range of $20 < We < 80$. The Reynolds number is fixed at $Re = 2000$.

Fig. 2 shows the calculated results of time evolution of droplet shape for $We = 20.2$ and $B = 0$. The condition corresponds to $V = 0.73$ m/s and $D = 2.7$ mm in the collision of water droplets at 20 °C. The droplet shape represents the surface of $\rho = 25$. After two droplets collide head-on, they form a disk-like droplet. Owing to the large curvature at the circumference of the disk-like droplet, there is a pressure difference between its inner and outer regions caused by surface tension. Thus, the disk contracts radially inward and pushes the liquid outward from its center forming a long cylinder with rounded ends. Then the cylinder oscillates until a spherical droplet is formed. This type of collision is called "coalescence collision".

Fig. 3 shows the calculated results for $We = 78.6$ and $B = 0$. The condition corresponds to $V = 2.9$ m/s and $D = 0.70$ mm in the collision of water droplets at 20 °C. The time evolution of droplet shape is similar to the previous case up to the formation of a long cylinder with rounded ends. In this case, however, the cylinder breaks into two major droplets and a smaller satellite droplet in the middle. This type of collision is called "reflexive separation collision". The fluid velocity fields at $y = L_y/2$ are shown in Fig. 4. The complicated gas flows outside the droplets as well as liquid flows inside the droplets are clearly found. The symmetry circular flows appear in the gas phase near the droplets.

Figs. 5 and 6 show the calculated results for $We = 79.5$ and $B = 0.5$. Since the two droplets collide at the high impact parameter, only a portion of them contacts directly, and the remaining portions of the droplets tend to move in the direction of their initial velocities and consequently stretch the region of the interaction. Finally, the droplet breaks into two major droplets and a smaller satellite droplet. This type of collision is called "stretching separation collision". It is found from Fig. 6 that the gas and liquid flows are so complicated around the droplets especially at $t^* = 8.00$. The computation time for this case required about 60 h on the AMD AthlonXP 1800+ PC machine.

We have calculated the binary droplet collisions for various Weber numbers and impact parameters, and classified the results into the above-mentioned three types of collision in the $We - B$ plane as shown in Fig. 7. It is seen that the reflexive separation collisions appear in the region of low impact parameters and high Weber numbers over a critical value, and the stretching separation collisions occur at high impact parameters. The coalescence collisions occur between the two regions. In the figure the theoretical prediction of the boundaries of the three types of collisions by using a simple energy balance analysis of Ashgriz and Poo [2] are also drawn. The present calculated results are in good agreement with the theoretical prediction, although the boundaries of the present results are shifted a little to the larger B.

The study of the mixing process during collisions is an important issue. By tracing fluid particles in two droplets, we investigate the mixing of fluids in two colliding droplets. The locations of the fluid particles every time step are calculated by using the fourth-order

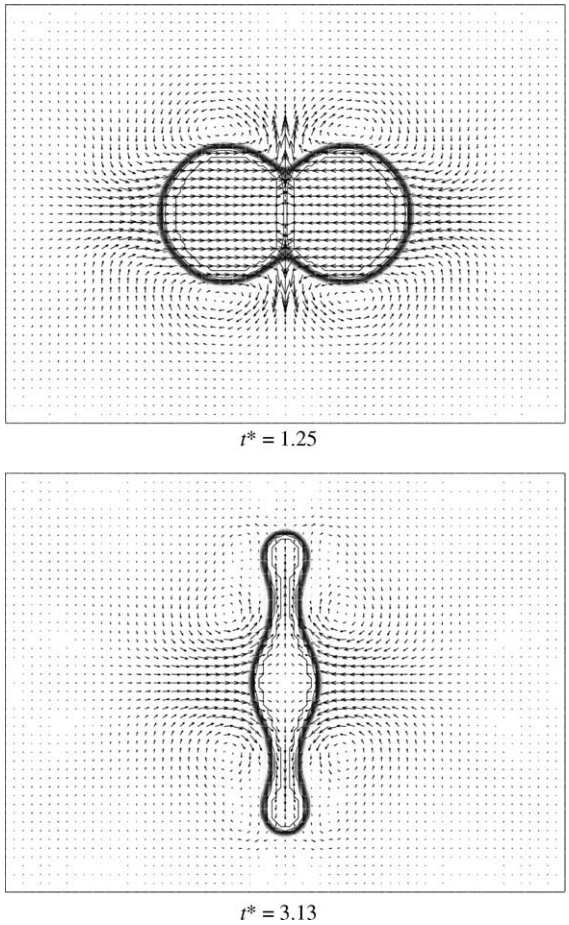

Fig. 4. Velocity vectors and density contours at $y = L_y/2$ for $We = 78.6$ and $B = 0$ ($t^* = tV/D$).

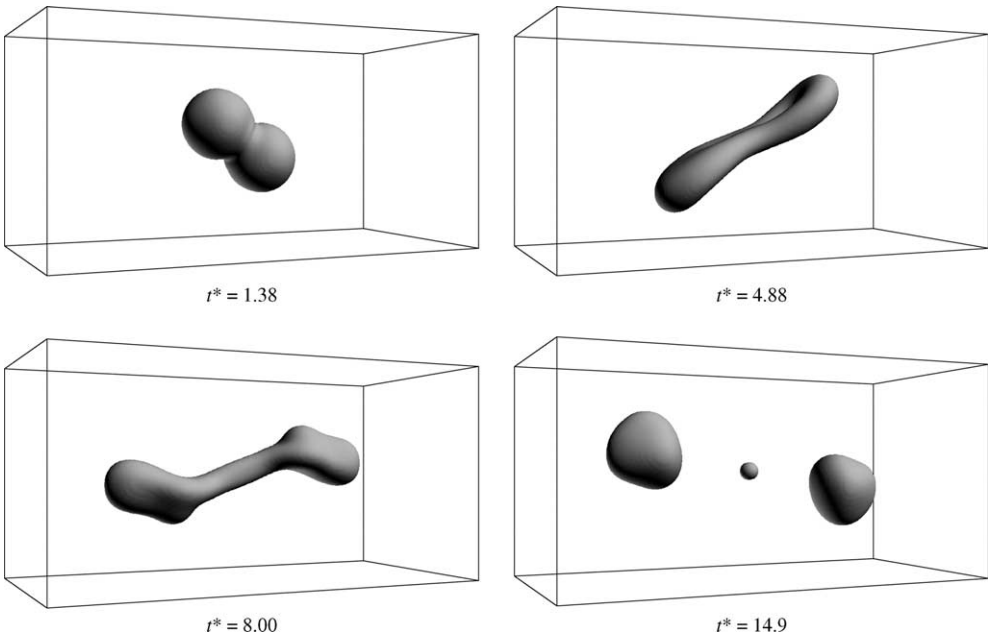

Fig. 5. Time evolution of droplet shape for $We = 79.5$ and $B = 0.5$ ($t^* = tV/D$).

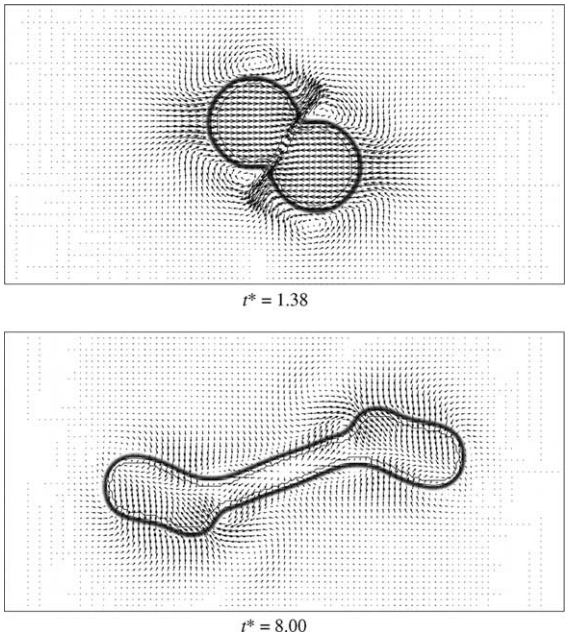

Fig. 6. Velocity vectors and density contours at $y = L_y/2$ for $We = 79.5$ and $B = 0.5$ ($t^* = tV/D$).

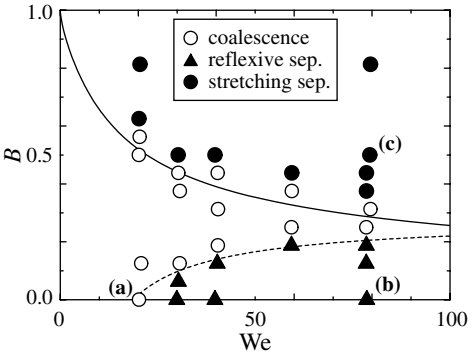

Fig. 7. Calculated results classified into three types of collisions. The solid and broken curves represent the theoretical prediction of the boundaries between three types of collisions [2]. (a) the case of Fig. 2; (b) the case of Figs. 3 and 4; (c) the case of Figs. 5 and 6.

Runge–Kutta method. Note that the particles going out of the droplets due to numerical errors are omitted in the calculation. Fig. 8 shows the calculated results for $We = 78.8$ and $B = 0.19$. In the figure the particles in $y \geqslant L_y/2$ are viewed from $y = -\infty$. Initially about 10,000 white and black particles are embedded in each droplet. After two droplets collide, the contact surface is stretched and rolls at $t^* = 3.13$ and 5.00, and then it is stretched in another almost perpendicular direction at $t^* = 7.50$ and 12.5. Finally, the droplet breaks into two partially mixed droplets. It is found that in this case the two different types of stretching process play an important role in the mixing of fluids in two colliding droplets. The mixing rate, which is defined here by the percentage of the number of the other colored particles in the total

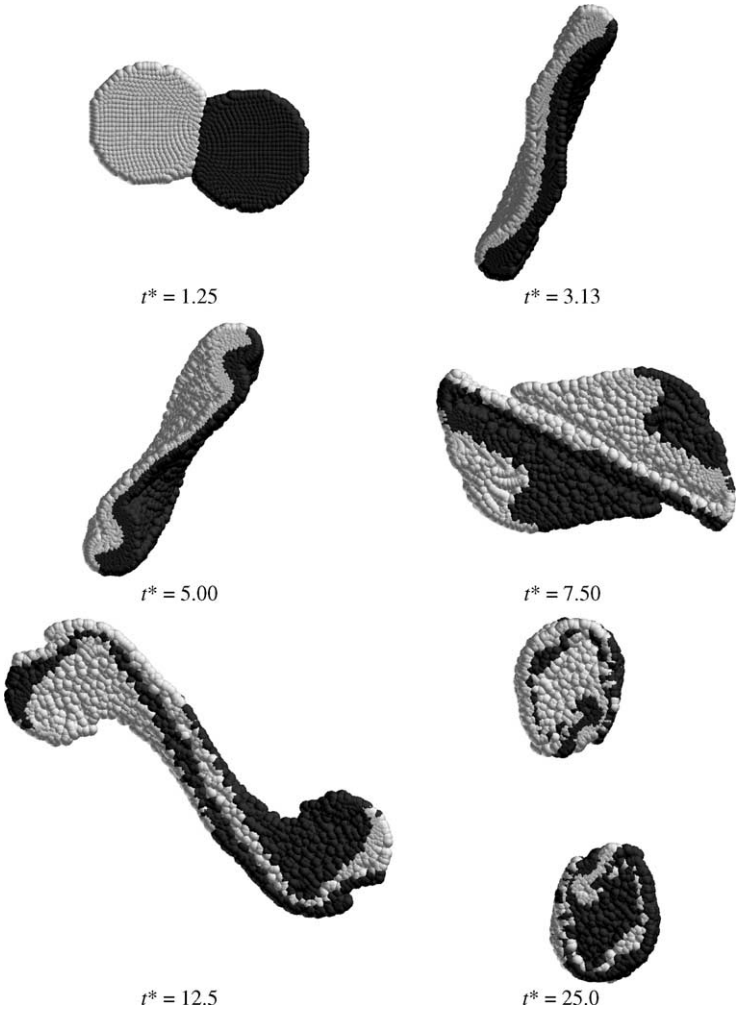

Fig. 8. Time evolution of tracer particles for $We = 78.8$ and $B = 0.19$ ($t^* = tV/D$). The particles in $y \geqslant L_y/2$ are viewed from $y = -\infty$.

number of particles in the separated major droplet, can be calculated by counting the number of the white and black particles in the separated droplet. For the upper droplet at $t^* = 25.0$ in this case, the mixing rate obtained is 29.9%. We have calculated the mixing rate for various impact parameters at $We \approx 80$, and the results are shown in Fig. 9. It is seen from Fig. 9 that the maximum mixing rate is obtained around $B = 0.2$ in the region of the reflexive separation.

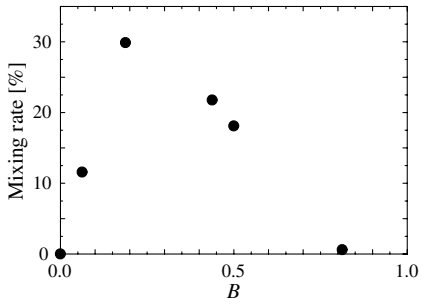

Fig. 9. Mixing rate versus B for $We \approx 80$.

4. Concluding remarks

We have presented a lattice Boltzmann method for two-phase fluid flows with large density ratios and applied the method to the simulations of binary droplet collisions for various Weber numbers and impact parameters. The calculated results can be classified into three types of collisions, namely coalescence, reflexive separation, and stretching separation collisions, which are in good agreement with the theoretical prediction. Also, we have illustrated the feature of mixing processes

during separating collisions by tracing colored particles embedded in the droplets. The approach is useful for the investigation of mixing processes during droplet collisions. For example, the mixing process of two unequal-size droplets is an interesting subject in future work. Moreover, it is known that there exist other types of binary droplet collisions under certain conditions, bouncing collision for low Weber numbers and shattering collision for high Weber numbers. We are presently trying to simulate these types of collisions by the present method. In addition, the simulation for higher density ratios is required in future work.

References

[1] G. Brenn, A. Frohn, Collision and merging of two equal droplets of propanol, Exp. Fluids 7 (1989) 441–446.
[2] N. Ashgriz, J.Y. Poo, Coalescence and separation in binary collisions of liquid drops, J. Fluid Mech. 221 (1990) 183–204.
[3] M. Orme, Experiments on droplet collisions, bounce, coalescence and disruption, Prog. Energy Combust. Sci. 23 (1997) 65–79.
[4] J. Qian, C.K. Law, Regimes of coalescence and separation in droplet collision, J. Fluid Mech. 331 (1997) 59–80.
[5] M. Rieber, A. Frohn, Navier–Stokes simulation of droplet collision dynamics, in: Proceedings of the 7th International Symposium on CFD Beijing, China, 1997, 520–525.
[6] F. Mashayek, N. Ashgriz, W.J. Minkowycz, B. Shotorban, Coalescence collision of liquid drops, Int. J. Heat Mass Transfer 46 (2003) 77–89.
[7] A.K. Gunstensen, D.H. Rothman, S. Zaleski, G. Zanetti, Lattice Boltzmann model of immiscible fluids, Phys. Rev. A 43 (1991) 4320–4327.
[8] X. Shan, H. Chen, Lattice Boltzmann model for simulating flows with multiple phases and components, Phys. Rev. E 47 (1993) 1815–1819.
[9] M.R. Swift, W.R. Osborn, J.M. Yeomans, Lattice Boltzmann simulation of nonideal fluids, Phys. Rev. Lett. 75 (1995) 830–833.
[10] X. He, S. Chen, R. Zhang, A lattice Boltzmann scheme for incompressible multiphase flow and its application in simulation of Rayleigh–Taylor instability, J. Comput. Phys. 152 (1999) 642–663.
[11] T. Inamuro, T. Miyahara, F. Ogino, Lattice Boltzmann simulations of drop deformation and breakup in simple shear flow, in: N. Satofuka (Ed.), Computational Fluid Dynamics 2000, pp. 499–504.
[12] T. Inamuro, R. Tomita, F. Ogino, Lattice Boltzmann simulations of drop deformation and breakup in shear flows, Int. J. Mod. Phys. B 17 (2003) 21–26.
[13] A.J. Chorin, Numerical solution of the Navier–Stokes equations, Math. Comput. 22 (1968) 745–762.
[14] T. Inamuro, M. Yoshino, F. Ogino, Accuracy of the lattice Boltzmann method for small Knudsen number with finite Reynolds number, Phys. Fluids 9 (1997) 3535–3542.
[15] T. Inamuro, N. Konishi, F. Ogino, A Galilean invariant model of the lattice Boltzmann method for multiphase fluid flows using free-energy approach, Comput. Phys. Commun. 129 (2000) 32–45.
[16] J.S. Rowlinson, B. Widom, Molecular Theory of Capillarity, Clarendon Press, Oxford, 1982, pp. 50–68.
[17] T. Inamuro, T. Ogata, S. Tajima, N. Konishi, A lattice Boltzmann method for incompressible two-phase flows with large density differences, J. Comput. Phys. (in press).